Magnetic rotational bands in ^{108}Sb

D. G. Jenkins,[1] R. Wadsworth,[1] J. Cameron,[2] R. M. Clark,[3] D. B. Fossan,[4] I. M. Hibbert,[1,*] V. P. Janzen,[5] R. Krücken,[3,†] G. J. Lane,[4,‡] I. Y. Lee,[3] A. O. Macchiavelli,[3] C. M. Parry,[1] J. M. Sears,[4] J. F. Smith,[4,§] and S. Frauendorf[6]
[1]*Department of Physics, University of York, Heslington, York Y01 5DD, United Kingdom*
[2]*Department of Physics and Astronomy, McMaster University, Hamilton, Ontario, Canada L85 4M1*
[3]*Lawrence Berkeley National Laboratory, Berkeley, California 94720*
[4]*Department of Physics, State University of New York at Stony Brook, Stony Brook, New York 11794-3800*
[5]*Chalk River Laboratories, AECL Research, Chalk River, Ontario, Canada K0J 1J0*
[6]*FZ Rossendorf, Postfach 510119, D-01314 Dresden, Germany*
(Received 29 June 1998)

High-spin states in ^{108}Sb were populated using the ^{54}Fe(^{58}Ni,3pn) reaction at a beam energy of 243 MeV and the subsequent γ decay was studied using the Gammasphere array. A new sequence of magnetic dipole transitions has been observed in addition to a previously known $M1$ band in ^{108}Sb. These bands may be interpreted, within the tilted axis cranking model as magnetic rotational bands with $\pi[g_{7/2}^2 \otimes (g_{9/2})^{-1}] \otimes \nu[h_{11/2}]$ and $\pi[h_{11/2} g_{7/2} \otimes (g_{9/2})^{-1}] \otimes \nu[(g_{7/2} d_{5/2})]$ configurations. [S0556-2813(98)01711-7]

PACS number(s): 21.10.Re, 23.20.Lv, 25.70.Gh, 27.60.+j

I. INTRODUCTION

Magnetic dipole bands, characterized by strong $M1$ transitions with relatively weak or absent $E2$ crossover transitions, have been observed in both the lead region [1–4] and, more recently, in the tin region [5,6]. These structures are readily distinguished from conventional rotational bands by their large $B(M1)$ values (several μ_N^2) indicating strong magnetic character. The small $B(E2)$ values [$B(E2) \simeq 0.1\, e^2$ b^2) [4]] associated with these structures indicate that they have low quadrupole deformation. Indeed, the distinctive properties of these bands strongly suggest that the majority of their aligned angular momentum is generated by a mechanism other than collective rotation. Such structures are believed to be examples of a phenomenon known as magnetic rotation for which a rotating magnetic dipole vector breaks the symmetry of the nucleus. The configurations and properties of these bands have been successfully described within the tilted axis cranking (TAC) model [7]. In this model, the proton and neutron angular momentum vectors, at the bandhead, are nearly perpendicular and the aligned angular momentum is generated by the shears mechanism, namely, the gradual alignment of these vectors with the total angular momentum vector, I, which is tilted at some angle, θ, with respect to the three axis (the symmetry axis of the nuclear density distribution). A definitive signature of this shears mechanism is that the $B(M1)$ values will decrease with increasing angular momentum, since they are proportional to the square of the perpendicular component of the magnetic dipole vector.

The TAC model [7–9] suggests that regular shears bands consisting of $M1$ transitions should exist in regions of low deformation and in proximity to shell closures such as $Z=50$ and $Z=82$. Such bands have recently been observed in ^{105}Sn [5] and ^{106,108}Sn [6]. The structures in ^{108}Sn were successfully interpreted in terms of the model. In the lighter isotopes, ^{105,106}Sn, however, the calculations had more limited success. The reasons for this were thought to result from the failure of the TAC model to fully include higher-order nuclear deformations (such as hexadecapole components) and possible proton-neutron interactions [6].

Other sequences of magnetic dipole transitions are known to exist in several neighboring nuclei in this mass region, for example, in ^{110,112}Sb [10,11], ^{108}Cd [12], ^{110}In and ^{111}In [13,14]. Although these structures have not yet been explicitly interpreted within the TAC model as examples of magnetic rotation (shears bands), they are likely to have a structure similar to the dipole bands in the tin isotopes. The present work provides an interpretation within the TAC model of a pair of magnetic dipole bands in an antimony nucleus.

II. EXPERIMENTAL DETAILS AND DATA ANALYSIS

Excited states in the nucleus ^{108}Sb were populated using the ^{54}Fe(^{58}Ni,3pn) reaction at a beam energy of 243 MeV. A ^{58}Ni beam accelerated by the 88-inch cyclotron at the Lawrence Berkeley National Laboratory was incident on a target composed of 600 μg/cm^2 enriched ^{54}Fe on a backing of 15.2 mg/cm^2 of gold. The full implementation of the *Gammasphere* array with 95 HPGe detectors was used to detect the resulting γ decay.

The data were unfolded and used to produce a γ-γ-γ cube, containing 2.1×10^{10} triples events, which was analyzed using the RADWARE analysis program, LEVIT8R [15]. This backed target data cube was explored for detailed infor-

*Present address: Oliver Lodge Laboratory, University of Liverpool, PO Box 147, Liverpool L69 3BX, U.K.
†Present address: Wright Nuclear Structure Laboratory, Physics Department, Yale University, New Haven, CT 06520.
‡Present address: Lawrence Berkeley National Laboratory, Berkeley, CA 94720.
§Present address: Nuclear Physics Group, Schuster Laboratory, University of Manchester, Brunswick Street, Manchester M13 9PL, U.K.

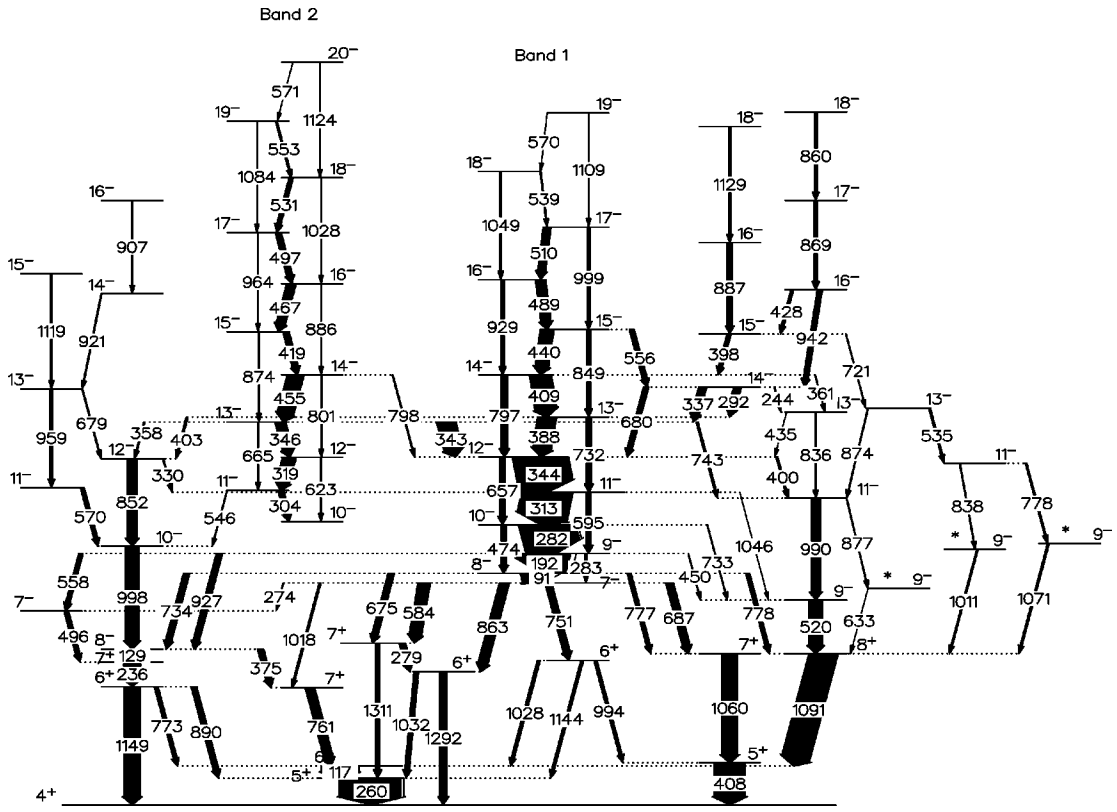

FIG. 1. Proposed level scheme for ^{108}Sb. The asterisks indicate known levels fed by decay from band 2 through as yet undefined decay paths.

mation about dipole bands in ^{108}Sb; the resulting level scheme is presented in Fig. 1. The backed target data were also unfolded and sorted into three two-dimensional matrices. In each case the data were unpacked into triples and gates were set on known $E2$ transitions (1149, 1292, 1091, 1311, and 1060 keV) at the bottom of the ^{108}Sb decay scheme in order to enhance the $3pn$ reaction channel. Matrices were created for ''all detectors'' against ''all detectors,'' ''all detectors'' against those detectors at 90 degrees and ''all detectors'' against those at forward ($<80°$) angles. The first matrix was used to extract $B(M1)/B(E2)$ ratios from the intensities of $M1$ transitions and their respective $E2$ crossover transitions. An angular correlation method was used to assign the multipolarity of previously unknown transitions, using the latter two matrices. These matrices were used to extract angular correlation ratios (R) from the ratio of the intensities of transitions in the forward angle matrix to those in the 90 degree matrix, after gating on known stretched quadrupoles on the ''all-detector'' axis. The values were normalized to take into account the difference between the numbers of detectors at forward angles and those at 90 degrees. Angular correlation ratios of known stretched dipole-stretched quadrupole transitions from this geometry have an average value of 0.85 ± 0.05, while those of known stretched quadrupole-stretched quadrupole transitions have an average value of 1.35 ± 0.05; these values are consistent with previous angular correlation measurements for ^{106,108}Sn taken from the same data set [6]. Possible ambiguities arising from this analysis are to a large extent removed in the present work by interpreting these measurements in conjunction with previously assigned levels. The results of these analyses are given in Table I.

III. EXPERIMENTAL RESULTS

A. Bands 1 and 2

A rotational band structure consisting of magnetic dipole transitions and crossover $E2$ transitions had been previously identified in ^{108}Sb and has been confirmed in the present work [see Fig. 2(a)] [16]. It has been possible to extend this band, labeled as band 1, by one further dipole transition, the 569.3 keV γ ray. In addition, a new magnetic dipole band has been observed in parallel to the first band, consisting of the 304.0, 319.0, 346.1, 455.4, 419.4, 467.1, 497.4, 530.5, 552.9, and 571.1 keV sequence with accompanying crossover transitions [see Fig. 2(b)]. The association of some of these transitions with the ^{108}Sb nucleus had been made previously [16]. The recognition of these transitions as a band and the band placement in the level scheme has been made possible by means of double gating in the γ-γ-γ cube and the requisite statistics. The placement of band 2 in the level scheme has been determined on the basis of two γ rays with energies of 342.9 and 797.6 keV, which connect this band with band 1. The latter of these two transitions forms a doublet with the 796.5 keV $E2$ crossover transition in band 1. A 358.0 keV transition also links band 2 to a known 12^- state on the left of the level scheme shown in Fig. 1. In addition, some of the intensity at the bottom of the band feeds out into the 9^- levels marked with asterisks on the right of the level scheme; however, it was not possible to identify the γ rays

TABLE I. γ-ray energies, intensities (relative to 259 keV γ ray), angular correlation ratios R, and spin assignments for the initial and final levels in ^{108}Sb. The angle set θ used in the angular correlation measurements includes all angles less than 80 degrees.

E_γ (keV)	I_γ (%)	$R=\frac{W(\text{all}-\theta)}{W(\text{all}-90)}$	Assignment $J_i^\pi \rightarrow J_f^\pi$
Band 1			
192.3(1)	30.0(4)	0.80(1)	$9^- \rightarrow 8^-$
281.6(2)	93.4(3)	0.85(1)	$10^- \rightarrow 9^-$
312.5(1)	76.3(4)	0.91(1)	$11^- \rightarrow 10^-$
344.4(1)	85.3(10)	0.86(2)	$12^- \rightarrow 11^-$
387.9(1)	36.8(2)	0.81(2)	$13^- \rightarrow 12^-$
408.9(1)	31.2(2)	0.90(4)	$14^- \rightarrow 13^-$
439.7(1)	21.5(3)	0.83(3)	$15^- \rightarrow 14^-$
488.6(1)	18.2(3)	0.97(6)	$16^- \rightarrow 15^-$
509.6(1)	11.6(4)	0.87(5)	$17^- \rightarrow 16^-$
538.5(2)	6.6(3)	0.93(8)	$18^- \rightarrow 17^-$
569.6(3)	1.5(4)	0.76(13)	$19^- \rightarrow 18^-$
Band 2			
304.0(1)	8.5(2)	0.68(6)	$11^- \rightarrow 10^-$
319.0(1)	19.6(3)	0.75(5)	$12^- \rightarrow 11^-$
346.1(1)	31.6(11)	0.88(8)	$13^- \rightarrow 12^-$
455.4(1)	35.3(3)	0.79(5)	$14^- \rightarrow 13^-$
419.4(1)	9.2(3)	0.71(6)	$15^- \rightarrow 14^-$
467.1(2)	13.8(3)	0.90(4)	$16^- \rightarrow 15^-$
497.4(4)	6.1(4)	0.96(11)	$17^- \rightarrow 16^-$
530.5(2)	4.3(4)	0.81(8)	$18^- \rightarrow 17^-$
552.9(2)	1.8(4)	0.92(10)	$19^- \rightarrow 18^-$
571.1(2)	1.2(3)	0.97(15)	$20^- \rightarrow 19^-$
Other transitions			
244.1(3)	2.0(2)	0.83(12)	$14^- \rightarrow 13^-$
273.9(1)	2.7(4)	0.52(12)	$7^- \rightarrow 7^-$
329.5(1)	2.8(4)	0.86(12)	$12^- \rightarrow 11^-$
342.9(3)	33.2(12)	0.93(4)	$13^- \rightarrow 12^-$
358.0(1)	5.7(3)	0.70(8)	$13^- \rightarrow 12^-$
361.0(3)	1.3(4)	0.78(16)	$14^- \rightarrow 13^-$
400.2(1)	6.4(3)	0.82(5)	$12^- \rightarrow 11^-$
403.0(1)	5.2(3)	0.75(6)	$13^- \rightarrow 12^-$
434.9(3)	1.7(2)	0.79(9)	$13^- \rightarrow 12^-$
495.8(3)	11.1(3)	0.58(6)	$7^- \rightarrow 7^+$
534.8(2)	3.7(3)	1.34(7)	$13^- \rightarrow 11^-$
546.2(2)	1.5(2)	0.98(9)	$11^- \rightarrow 10^-$
557.5(2)	7.5(4)	1.18(6)	$9^- \rightarrow 7^-$
632.6(2)	3.9(3)	0.76(8)	$9^- \rightarrow 8^+$
678.7(3)	2.3(4)	0.70(13)	$13^- \rightarrow 12^-$
743.2(3)	1.6(3)	1.08(14)	$13^- \rightarrow 11^-$
777.5(2)	3.6(4)	1.25(11)	$11^- \rightarrow 9^-$
835.5(2)	3.9(4)	1.23(7)	$13^- \rightarrow 11^-$
837.6(3)	2.1(3)	1.44(9)	$11^- \rightarrow 9^-$
874.0(3)	2.1(4)	1.53(18)	$13^- \rightarrow 11^-$
876.6(2)	3.0(4)	1.22(12)	$11^- \rightarrow 9^-$
907.0(4)	1.4(4)	1.62(19)	$16^- \rightarrow 14^-$
920.7(2)	2.3(3)	0.83(16)	$14^- \rightarrow 13^-$
1011.1(2)	3.1(3)	0.86(15)	$9^- \rightarrow 8^+$
1045.5(2)	2.3(3)	1.50(16)	$11^- \rightarrow 9^-$
1071.0(2)	5.2(4)	0.93(8)	$9^- \rightarrow 8^+$
1119.2(2)	2.7(3)	1.52(14)	$15^- \rightarrow 13^-$
1128.7(2)	2.5(3)	1.18(12)	$18^- \rightarrow 16^-$

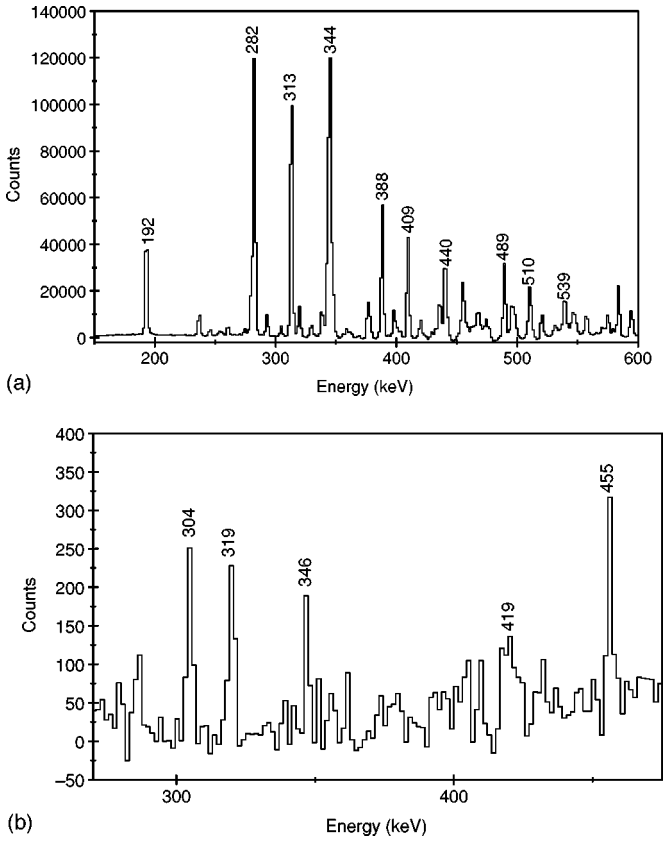

FIG. 2. (a) Spectrum showing band 1 double-gated on all combinations of in-band $M1$ transitions in the γ-γ-γ cube. Transitions within the band are labeled by their energies in keV. (b) Spectrum of band 2 double gated on the 1011 and 1091 keV γ rays. Transitions within the band are labeled by their energies in keV.

involved with the decay. Coincidence relations indicate that this decay is relatively weak and highly fragmented. These states are fed exclusively by band 2 and not band 1. It is possible therefore to obtain a clean double-gated γ-ray spectrum for band 2 [Fig. 2(b)].

Coincidence relationships strongly suggest that there is considerable crosstalk between the two bands over an extended spin range; however, no firm evidence has been obtained to demonstrate the existence of further interband transitions, either of $E2$ or $(J+1)\rightarrow J$ character, other than the two detailed above. Furthermore, despite an extensive search, no concrete evidence has been collected for direct links from the lowest three levels of band 2 into the low-lying spherical structure, apart from the 546.2 keV transition from the 11^- level. It is evident, therefore, from both intensity balances and coincidence relationships, that the majority of the decay from band 2 must be to band 1. It is clear that this decay proceeds only from band 2 to band 1 and not the reverse since it is possible to produce a clean spectrum of band 2 by gating on low-lying spherical structure [see Fig. 2(b)], while it is impossible to find a combination of similar gates to produce a spectrum of band 1 which does not also contain members of band 2. Given that states with the same J^π in each band are very similar in excitation energy and that no putative interband transitions have been observed, we believe that the necessary interband transitions, which are unobserved, must be of $J\rightarrow J$ character and of energies between

2 and 81 keV, and are, hence, highly converted. Such transitions would not be expected to be detected with the experimental setup used due to the relatively poor efficiency of the Gammasphere HPGe detectors at these energies. Indeed, the relatively intense 91 keV γ ray, known to be the bottom transition of band 1 [16], is unobserved in the present work.

An interesting feature of the two bands is that the respective 14^- and 12^- levels of each band are very close in excitation energy. Band 1 is weakly visible from the 15^- state upwards in a spectrum double gated in the cube on the 343/455 keV transitions, and band 2 is weakly visible in a spectrum double gated by the 409/388 keV transitions. This implies that there are unresolved transitions linking the 14^- and 13^- levels in the bands. The two 14^- levels in fact differ by 1.5 ± 0.3 keV and the 12^- levels are separated by 3.2 ± 0.3 keV.

B. Spherical states

In the present work, it has been possible to identify new transitions associated with the feedout of the magnetic dipole bands to both previously identified [16] and newly discovered spherical single-particle states. The new transitions added to the decay scheme in the present work are detailed in Table I. We have adopted the assumption from previous work [16] that the spin and parity of the ground state is 4^+; the assignment of all the other known levels is consistent with this assumption. There is, however, one inconsistency to be noted between the present work and the earlier level scheme. This involves the previous placement of the 836 keV transition in parallel to the 990 keV $11^- \rightarrow 9^-$ transition. In the present work this γ ray is placed above the 990 keV transition. From its angular correlation ratio, the 836 keV γ ray is identified as an $E2$ transition. This is confirmed by the existence of the 400 and 435 keV γ ray, which are crossed over by the 836 keV γ ray, and appear to be of stretched dipole character. These transitions must, in fact, be magnetic dipole transitions since the 400 keV γ ray feeds from a known 12^- level in band 1. The 13^- level above the 836 keV γ ray is fed by two stretched dipole transitions of 244 and 361 keV, from two previously identified 14^- levels.

Additional γ rays associated with the decay out of the magnetic dipole bands include the 403 and 358 keV transitions which feed out of the 13^- levels of bands 1 and 2 respectively, into the same 12^- level on the left of the level scheme. These appear to be of stretched dipole character. A 330 keV γ ray, also a stretched dipole, feeds from this 12^- level back into the 11^- level of band 1. An additional structure which may be associated with single-particle spherical states includes an irregular sequence consisting of the 495.8 and 557.4 keV transitions shown on the left of Fig. 1 feeding into a 7^+ level. This 495.8 keV transition forms a doublet with the 497.4 keV γ ray in band 2. The 557.4 keV transition is identified as an $E2$ transition. The measured ratio, $R = 0.58(6)$ for the 495.8 keV transition implies that it might be an unstretched dipole transition. Additional negative parity states have been identified with excitation energies around 2.5–3.5 MeV. The γ rays associated with the decay of these levels are detailed in Table I. Aside from the incorrect position of the 836 keV γ ray in the level scheme, the angular correlation ratios obtained for those additional transitions identified in the present work imply no further contradictions with previous spin assignments in the published level scheme [16].

IV. DISCUSSION

A dipole band with a bandhead spin of 7^- has been previously identified in ^{108}Sb and is a common feature of the heavier odd-odd antimony isotopes. For example, a similar structure has been observed in both ^{110}Sb [10] and ^{112}Sb [11]. For ^{108}Sb, a configuration of $\pi g_{9/2}{}^{-1} \otimes \nu h_{11/2}$ ($K = 5^-$) has been proposed [16] for the structure labeled in the present work as band 1. It is the intention of the present work to compare the configurations suggested by TAC calculations with the experimentally determined properties both of the previously known dipole band and the new dipole band observed in ^{108}Sb.

It is necessary, firstly, to summarize the experimental properties which are to be interpreted. In ^{108}Sb, two magnetic dipole bands of negative parity have been observed. Band 1 is the yrast band with a bandhead spin/parity of 7^- and excitation energy of 2.155 MeV. The second band, band 2, has an observed bandhead with spin/parity of 10^- and excitation energy of 2.749 MeV. These bands show a regular increase in spin with rotational frequency apart from a backbend in band 2 at the 13^- level. In addition, the relative intensity of band 2 to band 1 increases with increasing spin indicating that band 2 becomes yrast at high spin.

In the identification of TAC configurations, we use the commonly adopted letter code to denote quasineutrons where A, B, C, and D are the lowest positive parity $(g_{7/2}, d_{5/2})$ quasineutron levels and E, F, G, and H are the lowest negative parity $h_{11/2}$ quasiparticle levels (see Fig. 3). We denote the lowest $(g_{7/2}, d_{5/2})$ protons above the Fermi level as a, b, etc., and the lowest $h_{11/2}$ proton as e.

TAC calculations suggest that there are two plausible negative parity configurations which will be excited at an appropriate excitation energy and bandhead spin. The first suggested configuration is configuration 1 of $\pi[(g_{7/2}, d_{5/2})^2 \otimes (g_{9/2})^{-1}] \otimes \nu$[E], while configuration 2 is $\pi[h_{11/2}(g_{7/2}, d_{5/2}) \otimes (g_{9/2})^{-1}] \otimes \nu$[A].

A single-particle model was used for the protons since antimony is only one proton away from the $Z = 50$ closed shell, while a quasiparticle model was deemed more appropriate for the neutrons as ^{108}Sb has 57 neutrons where pairing effects will be important. The pairing constant used in the calculations was $\Delta_\nu = 1.1$ MeV and the chemical potential λ_ν was set to an appropriate value in order to preserve $N \simeq 57$.

Calculations carried out using the self-consistent total Routhian surface (TRS) model [17] with the proposed $\pi[(g_{7/2}, d_{5/2})^2 \otimes g_{9/2}{}^{-1}] \otimes \nu h_{11/2}$ configuration predict the existence of a minimum in the potential energy surface at a quadrupole deformation, $\epsilon_2 = 0.14$ and triaxiality parameter, $\gamma = 15°$. This contrasts with the minimum at $\beta_2 = 0.16$ (i.e., $\epsilon_2 = 0.15$) from conventional TRS calculations carried out in previous work [16]. The self-consistent deformation parameters were taken as the starting point for the TAC calculations. The deformation was minimized with respect to the total energy in the body-fixed frame by moving away stepwise in the ϵ_2-γ plane from these starting values until the

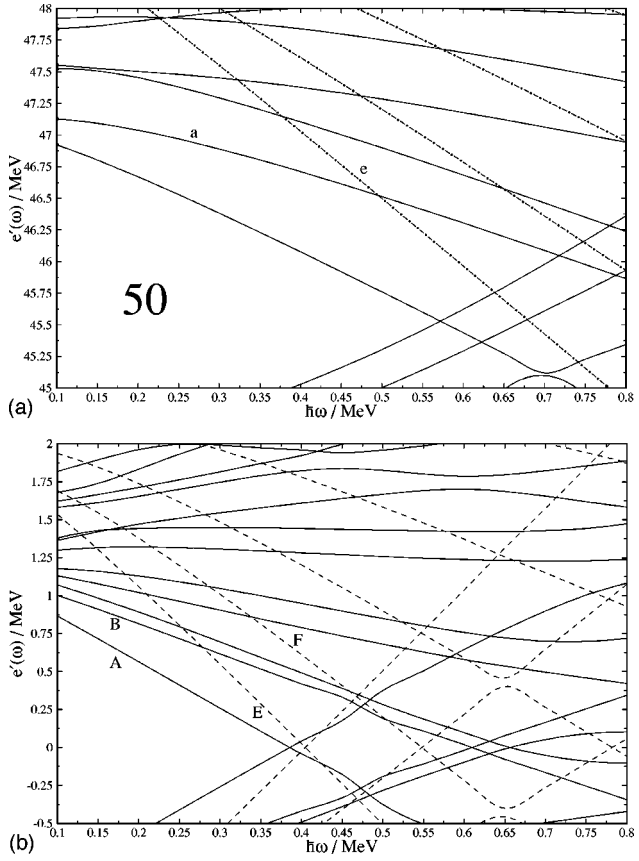

FIG. 3. (a) Single-particle Routhian plot for protons for ^{108}Sb. The $Z=50$ shell gap is marked. The lowest positive parity $(g_{7/2},d_{5/2})$ level above the Fermi level is the solid line labeled a. The lowest negative parity $h_{11/2}$ level is the dotted line labeled e. (b) Quasiparticle neutron Routhian plot for ^{108}Sb. The negative parity orbitals are indicated with dashed lines and labeled sequentially E and F. The positive parity levels are shown with solid lines and labeled as A, B, etc. with increasing energy. This plot was generated for a deformation of $\epsilon_2=0.11$ and $\gamma=10°$.

absolute minimum was found. This procedure was performed separately for the two configurations since the more steeply down-sloping $h_{11/2}$ proton orbital involved in configuration 2 might be expected to somewhat modify the deformation. The minimum for configuration 1 was found to correspond to a quadrupole deformation, $\epsilon_2=0.11$ and triaxiality parameter, $\gamma=30°$, while configuration 2 is associated with the same quadrupole deformation but a different triaxiality parameter, $\gamma=10°$. For simplicity, these deformations were treated as being unchanged with increasing rotational frequency.

TAC calculations, presented in Fig. 3(a), show that the proton $h_{11/2}$ orbital, labeled e, is relatively unfavorable for occupation until a rotational frequency of 0.4 MeV. At a rotational frequency of around 0.5 MeV, the proton $h_{11/2}$ orbital is seen to cross the $g_{7/2}$ orbital, labeled a, in the single-particle proton Routhian plot. The calculations indicate a linear increase in total angular momentum as a function of rotational frequency for both configurations apart from an up bend in the calculated curve for configuration 2, at a rotational frequency of around 0.45 MeV, which almost certainly arises from the alignment of the [EF] pair of $h_{11/2}$ neutrons [see Fig. 3(b)]. This is in qualitative agreement with the backbend observed in band 2 at a similar rotational frequency. Such an alignment is blocked for configuration 1 since the quasineutron orbital [E] is occupied.

Configuration 1 has a predicted bandhead excitation energy of 2.0 MeV whereas the bandhead of the structure generated by configuration 2 is predicted to lie at 2.4 MeV. These excitation energies compare favorably with the observed bandhead excitation energies (2.155, 2.749 MeV) of the two bands. The bandhead of the next most energetically favorable configuration, $\pi[(g_{7/2},d_{5/2})^2\otimes(g_{9/2})^{-1}]\otimes\nu[h_{11/2}(g_{7/2},d_{5/2})^2]$, which might arise from the breaking of a pair of $g_{7/2}$ neutrons, is predicted to lie at around 4.1 MeV. In view of the good agreement between the calculated and experimental excitation energies of the two bands and, more importantly, the fact that the two suggested configurations are the least energetic configurations, we restrict our subsequent analysis to these configurations.

An interesting feature of our calculations is that, at a rotational frequency of 0.4 MeV, both configurations being considered lead to a solution with a tilting angle, $\theta\sim25°$. This means that the predicted $B(E2)$ values will be very nearly equal since the value of $B(E2)$ is dependent on the quadrupole moment (deformation parameter) and tilting angle [18]:

$$B(E2,I\rightarrow I-2)=\frac{15}{128\pi}(eQ_o\ \sin^2\ \theta)^2. \tag{1}$$

The $B(M1)$ value is proportional to the square of the sum of the perpendicular components of the proton and neutron magnetic moments, given by the following semiclassical relationship, which is more readily expressed in terms of the proton angular momentum vector and the angle between this vector and the total angular momentum vector [19]:

$$B(M1,I\rightarrow I-1)=\frac{3}{8\pi}g_{\rm eff}^2 j_\pi^2\ \sin^2\ \theta_\pi. \tag{2}$$

This expression includes the effective gyromagnetic factor, $g_{\rm eff}=g_\pi-g_\nu$. The variables j_π and θ_π are the proton angular momentum component and the angle between the proton vector and the total vector (see Fig. 4). The relevant vector compositions of both configurations, at $\hbar\omega=0.4$ MeV, are given in Fig. 4. Figure 4(b) shows how the angular momentum vector ''blades'' are relatively asymmetric for configuration 2 at low frequency. At 0.5 MeV, the [EF] neutron pair are aligned and the blades become much more symmetric [Fig. 4(c)]. The tilting angle becomes much larger when this alignment is included and the ''shears'' reopen. Consideration of this figure demonstrates the considerable difference between the configurations 1 and 2; this geometric difference dictates that the $B(M1)$ values will differ between the two configurations. In fact, TAC calculations predict $B(M1)/B(E2)\sim10\ (\mu_N/eb)^2$ for configuration 1 and $\sim4\ (\mu_N/eb)^2$ for configuration 2 at low rotational frequency (<0.4 MeV). This, in turn, suggests that it ought to be possible to distinguish between the two configurations from their experimental $B(M1)/B(E2)$ ratios.

The TAC model has proved to be very successful in predicting the $B(M1)/B(E2)$ ratios for ^{108}Sn [6]. For the more weakly deformed nuclei, ^{105,106}Sn, however, the model was

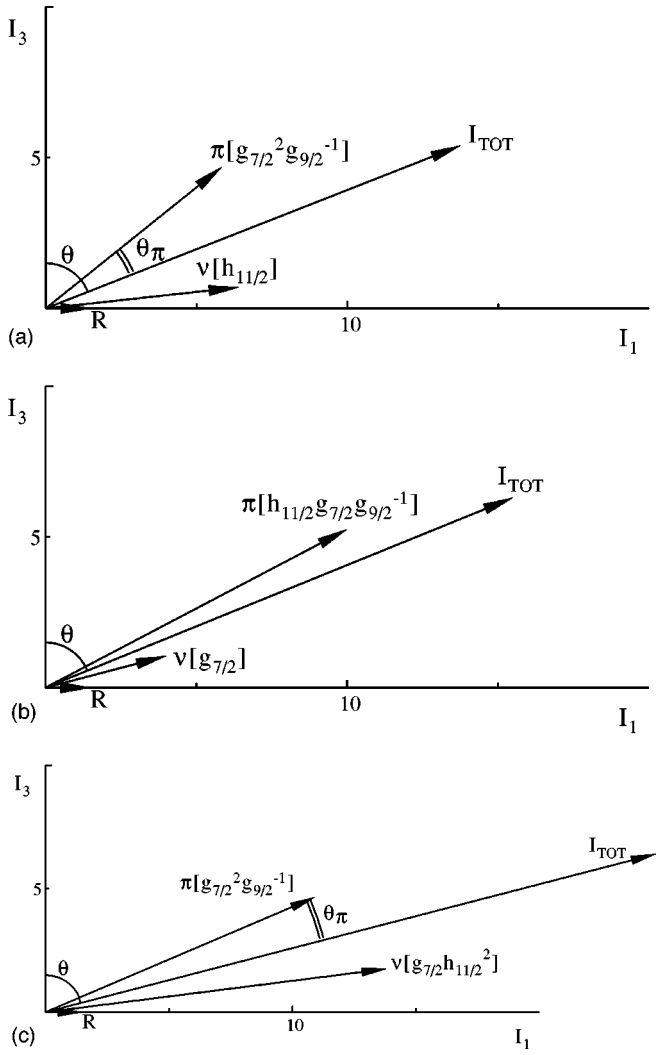

FIG. 4. Vector composition (derived from TAC calculations and shown to scale) of the total angular momentum, demonstrating the origin of the difference in $B(M1)$ values between the two configurations, for (a) Configuration 1—$\pi[g_{7/2}{}^2\otimes(g_{9/2})^{-1}]\otimes\nu[h_{11/2}]$ at a rotational frequency of 0.4 MeV, (b) Configuration 2—$\pi[h_{11/2}g_{7/2}\otimes(g_{9/2})^{-1}]\otimes\nu[g_{7/2}]$ at 0.4 MeV, (c) Configuration 2 at 0.5 MeV after the alignment of the [EF] neutrons.

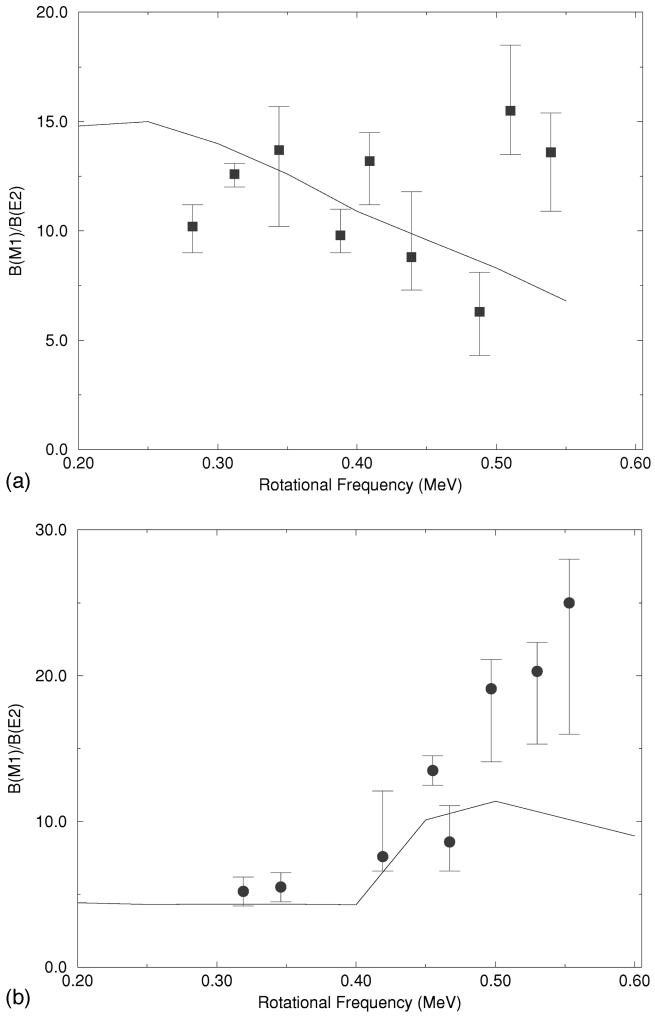

FIG. 5. Comparison of calculated and experimental $B(M1)/B(E2)$ values for ^{108}Sb as a function of rotational frequency for (a) band 1 (squares) and the calculation for configuration 1, $\pi[g_{7/2}{}^2\otimes(g_{9/2})^{-1}]\otimes\nu[h_{11/2}]$, (b) band 2 (circles) and the calculation for configuration 2, $\pi[h_{11/2}g_{7/2}\otimes(g_{9/2})^{-1}]\otimes\nu[g_{7/2}]$.

somewhat less successful in modeling the experimental $B(M1)/B(E2)$ ratios [5,6]. The under prediction, by an order of magnitude, has been attributed to the overestimation in the calculations of the quadrupole deformation in these near-spherical nuclei, which may arise from either the failure to take into account the hexadecapole degree of freedom or from other weaknesses of the TAC model such as the incomplete inclusion of proton-neutron interactions.

Obtaining experimental $B(M1)/B(E2)$ ratios for ^{108}Sb is complicated by the degeneracy of several of the $E2$ crossover transitions with transitions in the highly fragmented decay out of the magnetic rotational bands (see Table I and Fig. 1). This, combined with the interaction of the bands in the region around the 13^- level further complicates the analysis. Despite these difficulties, however, it has been possible to extract $B(M1)/B(E2)$ ratios for the respective bands. The somewhat large error bars for some data points reflect the difficulties discussed above. These are shown in Fig. 5 along with the predictions for the two configurations. The features to be noticed in this figure are the good agreement of the $B(M1)/B(E2)$ values for band 1 with those predicted for configuration 1, suggesting that band 1 has the configuration, $\pi[(g_{7/2},d_{5/2})^2\otimes(g_{9/2})^{-1}]\otimes\nu[\mathrm{E}]$. The increase in $B(M1)/B(E2)$ values for the top two experimental points may be caused by an [FG] neutron alignment predicted to occur at a rotational frequency of around 0.55 MeV. For band 2, the $B(M1)/B(E2)$ values at the bottom of the band are close to those predicted for configuration 2 and the sharp rise in the $B(M1)/B(E2)$ ratios at around 0.45 MeV, which is mostly probably caused by the alignment of the [EF] neutron pair, appears to be reproduced qualitatively by configuration 2. The reasonable agreement between the data and the calculations supports the assignment of the $\nu[\mathrm{A}]\otimes\pi[h_{11/2}g_{7/2}\otimes(g_{9/2})^{-1}]$ configuration to band 2.

V. CONCLUSION

In conclusion, two magnetic dipole bands have been observed in ^{108}Sb. The suggested configurations for these bands produce TAC solutions which show good agreement

with the experimental bands. The two configurations are distinguishable, in principle, on the basis of their associated $B(M1)/B(E2)$ ratios. $B(M1)/B(E2)$ ratios extracted from the data set agree well with those predicted by TAC calculations and support the proposed configuration assignments. The successful calculations carried out in the present work lend support to the validity of the description of magnetic dipole bands in this region in terms of the tilted axis cranking model.

ACKNOWLEDGMENTS

We would like to thank the staff of the 88-Inch Cyclotron and A. Lipski for making the targets used. This work was supported in part by the U.S. NSF and Department of Energy under Contract No. DE-AC03-76SF00098, the UK EPSRC, AECL and the Canadian NSERC. C.M.P. acknowledges support from the University of York. D.G.J. acknowledges support from the EPSRC.

[1] R. M. Clark *et al.*, Nucl. Phys. **A562**, 121 (1993).
[2] G. Baldsiefen *et al.*, Nucl. Phys. **A574**, 521 (1994).
[3] M. Neffgen *et al.*, Nucl. Phys. **A595**, 499 (1995).
[4] R. M. Clark *et al.*, Phys. Rev. Lett. **78**, 1868 (1997).
[5] A. Gadea *et al.*, Phys. Rev. C **55**, R1 (1997).
[6] D. G. Jenkins *et al.*, Phys. Lett. B **428**, 23 (1998).
[7] S. Frauendorf, Nucl. Phys. **A557**, 259c (1993).
[8] S. Frauendorf, J. Meng, and J. Reif, in *Proceedings of the Conference on Physics from Large γ Ray Detectors, Berkeley, 1994* (Report No. LBL-35687), Vol. II, p. 52.
[9] S. Frauendorf, in *Proceedings of Workshop on Gammasphere Physics, Berkeley, 1995* (World Scientific, Singapore, 1996).
[10] G. J. Lane *et al.*, Phys. Rev. C **55**, R2127 (1997).
[11] G. J. Lane *et al.*, Phys. Rev. C **58**, 127 (1998).
[12] I. Thorslund *et al.*, Nucl. Phys. **A564**, 285 (1993).
[13] C. J. Chiara (private communication).
[14] P. Vaska *et al.*, Phys. Rev. C **57**, 1634 (1998).
[15] D. C. Radford, Nucl. Instrum. Methods Phys. Res. A **361**, 297 (1995).
[16] J. Cederkäll *et al.*, Nucl. Phys. **A581**, 189 (1995).
[17] W. Satuła and R. Wyss, Phys. Scr. **T56**, 159 (1995).
[18] S. Frauendorf and J. Meng, Z. Phys. A **356**, 264 (1996).
[19] A. O. Macchiavelli, R. M. Clark, M. A. Deleplanque, R. M. Diamond, P. Fallon, I. Y. Lee, F. S. Stephens, and K. Vetter, Phys. Rev. C **57**, R1073 (1998).